

## VLF Electric and Magnetic Fields Observed with the Javelin 8.45 Sounding Rocket

STANLEY D. SHAWHAN<sup>1</sup> AND DONALD A. GURNETT

*Department of Physics and Astronomy  
University of Iowa, Iowa City, Iowa 52240*

A rocket VLF experiment flown from Wallops Island to an altitude of 763 km is described, and the experiment results are discussed. A noise band between about 7.5 and 30 kHz was observed with both the electric and magnetic receivers. The field geometry of this noise suggests that the noise is propagating perpendicular to the geomagnetic field and that the lower cutoff frequency may be the lower hybrid resonance frequency. Intense noise bursts below 1 kHz were observed on the electric antennas below 500-km altitude during both the upgoing and downgoing portions of the flight, but not on the loop antennas. The precession and spin modulation of this noise is not consistent with an interpretation of these noise bursts as being due to long wavelength electrostatic waves in the surrounding plasma. We suggest that this electric antenna noise may be generated by the motion of the payload. The magnitude of the electric antenna impedance varied from a minimum of about 150 kilohms at 350-km altitude to about 600 kilohms at apogee. A large phase perturbation, usually inductive, was observed at altitudes below about 500 km whenever the antenna was aligned nearly parallel to the geomagnetic field. The electric field signal from the nosecone transmitter was attenuated much more rapidly than the magnetic field.

### INTRODUCTION

This paper describes a very-low-frequency (VLF) electric and magnetic fields experiment flown on the Javelin 8.45 UI sounding rocket from Wallops Island, Virginia, and summarizes the amplitudes and frequency spectra of the electric and magnetic fields observed during the flight.

The scientific objectives of this experiment were to determine the amplitude and frequency spectra of naturally occurring electric and magnetic fields in the frequency range from 30 Hz to 10 kHz using three magnetic loop antennas and a variety of electric dipole antennas and to investigate the performance of the electric dipole antennas by comparing the natural signals from the different electric antennas and by measuring the mutual impedance of one pair of dipoles and the mutual coupling to the other antenna elements. Because much of the same instrumentation is to be flown on the Injun 5 satellite [Gurnett *et al.*, 1966], this experiment had the technical objective of evaluating the mechanical and electrical systems in the flight environment.

### INSTRUMENTATION

The payload instrumentation consists of six antennas and seven receivers for the detection of VLF electric and magnetic fields, an impedance measurement for determining the dipole antenna impedance, a nosecone VLF transmitter, and the battery power, telemetry, and pyrotechnic support systems.

A block diagram of the VLF experiment instrumentation is shown in Figure 1. The  $E_x$  and  $E_y$  electric antennas, parallel to the  $x$  and  $y$  axis, respectively, are of the type described by Storey [1965]. These electric dipole antennas consist of two spherical aluminum antenna elements 15.3 cm in diameter with a center-to-center separation of 3.16 meters. The booms supporting these antenna elements are insulated from the payload and the spheres and are coated with a nonconducting paint to insulate the booms from the surrounding plasma. Spring-loaded joints allow folding the booms for storage in the nosecone during launch and provide energy for erection. Two different types of spherical electric antenna elements were used to compare their performance in a plasma; solid conducting spheres in the  $E_y$  system and 60% transparent, nonconducting spheres on the  $E_x$  system. Also, the  $E_y$  antenna elements were

<sup>1</sup> Present address: Royal Institute of Technology, Stockholm 70, Sweden.

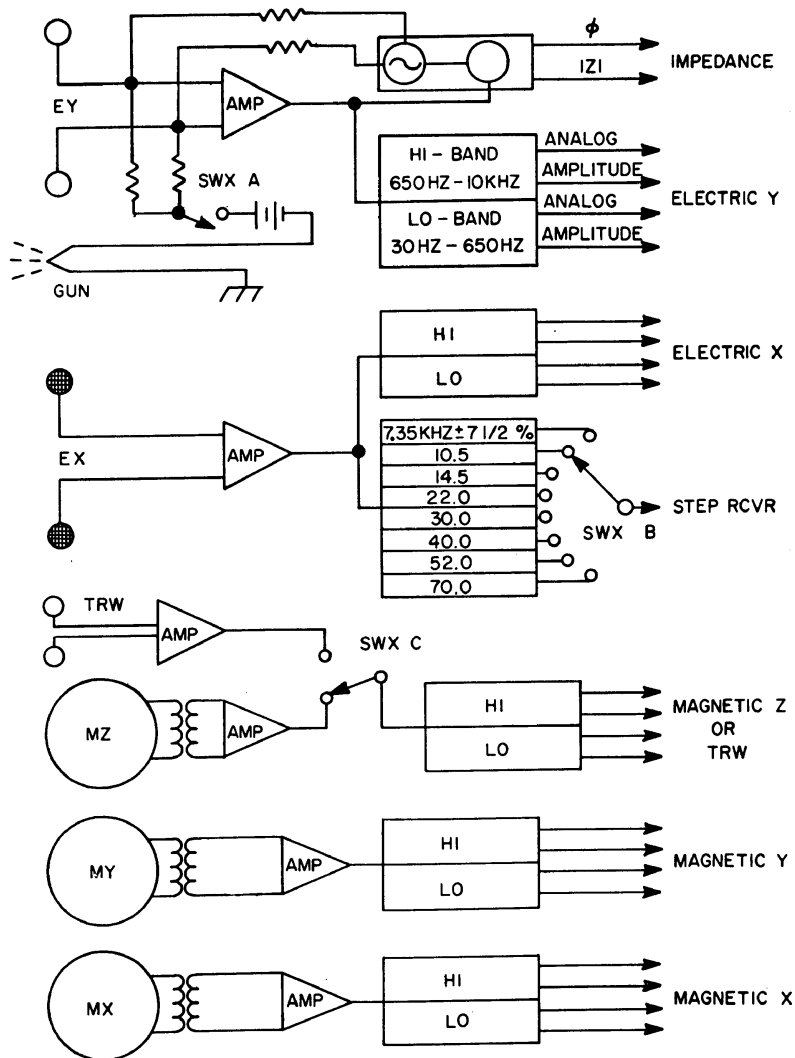


Fig. 1. Block diagram of the Javelin 8.45 experiment.

biased with  $1\text{ }\mu\text{amp}$  (20 volts across 20 megohms) of current to reduce the plasma sheath around the antenna. The electrons collected from the plasma by this bias were returned to the plasma by the collimated hot filament labeled 'gun' in Figure 1. Swx A turned the biasing system 'on' for 32 seconds and 'off' for 32 seconds during the flight.

Inside of each sphere is a unity gain amplifier that acts as an impedance transformer for driving the booms to cancel the sphere-boom capacity and for driving the input coaxial cable to the differential amplifier. The input impedance of the unity gain amplifiers can be repre-

sented by a 20-megohm resistor in parallel with a 10-pf capacitor. As shown in Figure 1, the unity gain outputs from the dipole antennas drive a differential amplifier located within the payload. The output of the differential amplifier for the *Ey* antenna is fed into two circuits: the antenna impedance measurement and the wideband VLF receiver.

To interpret the ac electric field strengths for VLF waves from the observed voltage on the electric antenna and to observe large changes in antenna impedance at natural resonance frequencies, the impedance of the *Ey* antenna is measured. A constant amplitude ac current

source ( $I = 0.05 \mu\text{amps rms}$ ) with a frequency that decreases exponentially from 20 kHz to 20 Hz is used to differentially drive the  $E_y$  antenna elements. The ratio of the voltage amplitude  $V$  from the differential amplifier to the current  $I$  gives the magnitude of the antenna impedance  $|Z| = V/I$ , and a comparison of the voltage and current waveforms gives the phase  $\phi$  of the impedance. Every eight seconds the impedance measurement is made with the frequency sweep taking 1.5 seconds (0.5 second/decade). The magnitude measurement has a dynamic range of 100 kilohms to 10 megohms, and the phase measurements has a dynamic range of  $\pm 90^\circ$ .

The  $E_y$  differential amplifier also feeds the electric Y wideband receiver as shown in Figure 1. The wideband receiver consists of two bandpass filters, each followed by a compressor amplifier. These bandpass filters provide a low-frequency band of 30 to 650 Hz and a high-frequency band of 650 Hz to 10 kHz, which are independent of each other. The compressor amplifiers preserve frequency information over the channel bandwidth and have a 40-db dynamic range to provide the wideband analog signal. Also a dc amplitude voltage proportional to the total rms amplitude in the band over an 80-db dynamic range is provided. The sensitivity of each band is approximately 20  $\mu\text{volts rms}$  potential difference between the spheres. All five wideband receivers have this same bandpass filter-compressor amplifier system with analog and amplitude outputs for each band as indicated by 'lo,' for the 30-650 Hz band, and 'hi,' for the 650 Hz to 10 kHz band, in Figure 1.

Except for the orientation and sphere type, the  $E_x$  antenna system and differential amplifier are the same as the  $E_y$  system. This  $E_x$  system is not, however, biased. The differential amplifier feeds the electric X wideband receiver (identical to the electric Y receiver) and an eight channel step frequency receiver. The center frequencies of the eight-step frequency receiver channels are 7.35, 10.5, 14.5, 22.0, 30.0, 40.0, 52.5, and 70.0 kHz with bandwidths of  $\pm 7\frac{1}{2}\%$ .

Switch B in Figure 1 connects each filter sequentially to a circuit that produces a voltage proportional to the logarithm of the noise power in that channel. All channels are sampled every

0.31 second. This step receiver has a noise level of  $10^{-18} \text{ volt}^2 \text{ Hz}^{-1}$  and a dynamic range of 60 db.

A third electric dipole antenna and preamplifier system was provided by F. L. Scarf of TRW Systems for comparison with the  $E_y$  and  $E_x$  electric receivers. It is labeled 'TRW' in Figure 1. This dipole antenna consists of two spherical wire cages 6.02 cm in diameter with a center-to-center spacing of 48.2 cm. The TRW dipole is located at the top of the payload in a plane parallel to  $E_y$  and  $E_x$  and at  $45^\circ$  to  $E_y$  and  $E_x$ . The TRW antenna preamplifier system is similar to the electric antenna flown by Scarf [1967] on the OV3-3 satellite. The TRW preamplifier was subcommutated with the magnetic Z preamplifier by switch C (Figure 1) being 'on' for 8 seconds and 'off' for 8 seconds. The TRW preamplifier sensitivity was 30  $\mu\text{volts}$  in the lo band and 7  $\mu\text{volts}$  in the hi band. The input impedance of the TRW preamplifier can be represented by a 500-megohm resistance in parallel with a 100-pf capacitance.

The three orthogonal loop antennas, labeled  $M_x$ ,  $M_y$ , and  $M_z$  in Figure 1, run between the four booms. The  $M_z$  loop is a square loop with its axis parallel to the  $z$  axis and has an area of 1.6 meters<sup>2</sup>. The  $M_x$  and  $M_y$  loops are triangular loops that run from the top of the payload to the booms and through the payload with their axis parallel to the  $x$  and  $y$  axis, respectively. The areas of the  $M_x$  and  $M_y$  loops are 0.8 meter<sup>2</sup>. Each loop consists of three turns of #14 stranded copper wire and is electrostatically shielded. The loops are matched to the preamplifiers by a transformer with a 200:1 turns ratio. All three magnetic receivers have hi-lo filters and compressor amplifiers similar to the electric receivers. The sensitivities of the magnetic receiver hi and lo bands are approximately 0.5 and 3 m $\gamma$ , respectively (1 m $\gamma = 10^{-8}$  gauss).

All of the data were transmitted by a wide deviation ( $\pm 275 \text{ kHz}$ ) FM/FM telemetry system. The hi and lo analog outputs were mixed for each receiver and transmitted as a baseband and four FM subcarrier channels. The ten amplitude outputs from the five wideband receivers and the eight amplitude outputs from the step receiver were commutated onto one IRIG FM subcarrier. Another subcarrier provided the triaxial magnetometer data, and a

third subcarrier provided payload performance data.

To study VLF wave propagation from a known source, a VLF transmitter was installed in the nosecone. The antennas for this transmitter consisted of a 62-turn loop antenna 0.5 meter in diameter and an electric dipole antenna 1 meter tip-to-tip. These antennas were pulsed every 2 seconds with a 0.5-second sine wave burst that alternated between 2 and 8 kHz. The peak-to-peak current in the loop antenna was 4.2 amps, and the peak-to-peak voltage applied to the electric antenna was 320 volts.

### PAYLOAD PERFORMANCE

The Javelin 8.45 sounding rocket, launched at 07h 38m September 21, 1967, carried the payload to an altitude of 763 km and provided field, about 3.0. From the spin modulation of the payload to an altitude of 763 km and provided data for 15.5 minutes. Analysis of the triaxis magnetometer data after the booms opened indicates that the payload had a spin period of 5.45 seconds (11.0 rpm) about the payload  $z$  axis and a precession period of 17.7 seconds (3.39 rpm). The precession cone of the  $z$  axis was  $27^\circ$  half-angle. The orientation of the precession cone was determined from the magnetometer data and from the  $\mathbf{V} \times \mathbf{B}$  potential difference measurement with the  $Ey$  antenna. The coordinates used for analysis of the orientation consisted of the geomagnetic  $\mathbf{B}$  field, the projection  $\mathbf{V}_\perp$  of the payload velocity vector into a plane perpendicular to the geomagnetic field, and the  $\mathbf{E} = \mathbf{V} \times \mathbf{B}$  electric field. Shown in Figure 2 are the polar,  $\theta_z$ , and azimuthal,  $\phi_z$ , angles of the  $z$  axis near the beginning (300 km, upgoing) and end (300 km, downgoing) of the flight. Since the precession cone stays fixed in space and the  $\mathbf{B}$  and  $\mathbf{V}_\perp$  directions change slowly, the orientation at intermediate altitudes can be estimated from Figure 2 by interpolation. It should be noted from Figure 2 that once per precession period the  $z$  axis is nearly perpendicular to the geomagnetic field.

With two exceptions, the payload operated satisfactorily throughout the flight. One exception was the electron gun. Either the filaments or some of the associated wiring failed during launch because no bias current was obtained for the spheres. Thus, throughout the flight the spheres were unbiased, and it was not possible

to compare the biased and unbiased operation of the  $Ey$  antenna.

The second exception was the nosecone separation velocity indicator. According to the separation velocity indicator, the nosecone separated but was apparently decelerated to zero velocity by the drag on the ribbon that gave the separation velocity indications. However, the amplitude of the radio pulses emitted by the VLF nosecone transmitter did decrease after the antenna booms were fully opened. This amplitude decrease indicates that the ribbon apparently broke and the nosecone did move away from the payload. Also two objects were resolved by the tracking radar. This failure affects only the interpretation of the nosecone transmitter results.

### SUMMARY OF EXPERIMENTAL RESULTS

In this section all of the experimental results from the VLF receivers, the impedance measurement, and the nosecone transmitter are summarized. Detailed analyses of the noise phenomena observed are discussed in the following two sections.

*A. Wideband and step receiver results.* The frequency spectra of the electric and mag-

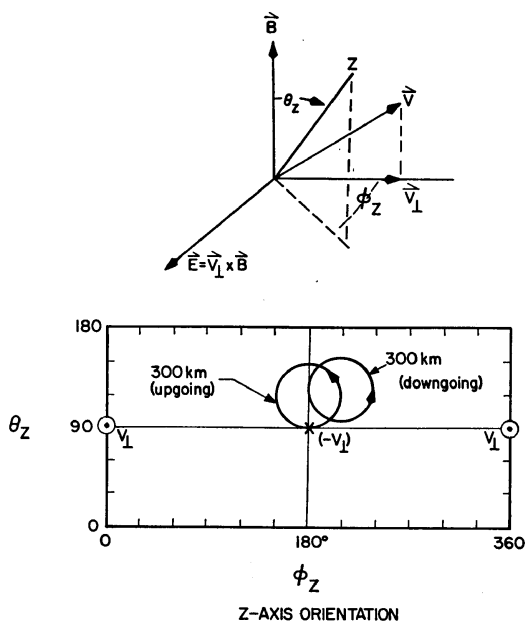


Fig. 2. Orientation of the  $z$  axis relative to the geomagnetic field  $\mathbf{B}$ , the perpendicular component of the velocity vector  $\mathbf{V}_\perp$ , and the  $\mathbf{V} \times \mathbf{B}$  electric field.

netic fields observed during the flight are summarized in Figure 3. Shown in Figure 3 are the frequency-time spectrograms of signals from the analog output of one electric receiver ( $Ex$ ) and from one magnetic receiver ( $My$ ). The frequency scale is from 0 to 10 kHz, and the time scale is in minutes after launch. Also shown are representative frequency-amplitude spectra from the step frequency receiver at six selected altitudes. The amplitude scale is logarithmic in units of voltage spectral density from  $10^{-13}$  to  $10^{-6}$  volts<sup>2</sup> Hz<sup>-1</sup>. A summary of the maximum and minimum field strengths from the amplitude outputs of the magnetic, electric, and TRW receivers is given in Table 1 at 100-km altitude intervals, each maximum and minimum value being within the interval of  $\pm 50$  km about the given altitude. The electric antenna amplitudes are the rms potential difference between the antenna terminals. These antenna voltages can be interpreted as electric fields in the plasma only in so far as the sheath impedance can be considered negligible in comparison with the preamplifier input impedance (see the discussion of antenna impedance results).

Two principal types of VLF noise phenomena are seen in Figure 3: a high-frequency noiseband above about 7 kHz, and low-fre-

quency noise bursts below 1 kHz. Broadband noise extending from about 7 to 30 kHz is observed throughout the flight on both the electric and magnetic antennas. As can be seen from Figure 3 the lower frequency limit of this noise band varies systematically with altitude, reaching a minimum frequency of approximately 7.5 kHz at apogee. The step receiver data show that the upper frequency limit, at about 30 kHz, also varies systematically with altitude, decreasing in frequency with increasing altitude. The magnetic hi-band signal strength, principally due to the high-frequency noise band, tends to increase slightly toward apogee to a value of about 10 mV. The electric hi-band field strength has strong spin modulation with maximum amplitudes of 8–12 mV throughout the flight. From the step receiver the peak electric field spectral density is approximately  $10^{-8}$  volts<sup>2</sup> m<sup>-2</sup> Hz<sup>-1</sup>, and the corresponding magnetic field spectral density is approximately  $4 \times 10^{-8}$   $\gamma^2$  Hz<sup>-1</sup> (2.5-kHz bandwidth). This high-frequency noise band is discussed further in the next section.

Intense electric antenna noise with frequencies below about 1 kHz was detected by both the Storey-type electric antennas and by the TRW electric antennas. This noise occurred primarily below about 500-km altitude, from 2

TABLE 1. Summary of Wideband Receiver Signal Strengths\*

Altitude, km	Low Bands (30–650 Hz)						High Bands (0.65–10 kHz)					
	Magnetic Z, mV		Electric X <sup>†</sup> , mV		TRW, <sup>†</sup> mV		Magnetic Y, mV		Electric X, <sup>†</sup> mV		TRW, <sup>†</sup> mV	
	Max	Min	Max	Min	Max	Min	Max	Min	Max	Min	Max	Min
300 up	10.0	7.0	20.0	10.0	8.0	2.5	10.0	7.0	7.0	1.5	1.0	0.50
400 up	15.0	5.0	5.0	0.3	4.0	0.2	10.0	7.0	4.0	0.5	0.25	0.06
500 up	18.0	6.0	4.0	0.1	3.0	0.05	12.0	8.0	8.0	0.8	0.10	0.08
600 up	15.0	4.0	1.5	0.06	1.0	0.04	12.0	8.0	12.0	1.0	0.09	0.06
700 up	8.0	6.0	0.4	0.06	0.3	0.04	15.0	9.0	12.0	1.0	0.10	0.07
764 apogee	10.0	5.0	0.3	0.06	0.08	0.03	12.0	8.0	9.0	1.0	0.07	0.05
700 down	8.0	6.0	0.4	0.07	0.10	0.04	20.0	8.0	12.0	1.5	0.09	0.07
600 down	10.0	6.0	0.5	0.07	0.10	0.04	20.0	8.0	10.0	2.0	0.10	0.08
500 down	9.0	7.0	2.0	0.08	1.0	0.3	12.0	6.0	7.0	1.0	0.12	0.08
400 down	7.0	5.0	4.0	0.10			9.0	5.0	4.0	1.0	0.20	0.09
300 down	8.0	6.0	9.0	0.15	2.0	0.06	7.0	5.0	3.0	0.2	0.40	0.10
200 down	9.0	7.0	0.3	0.06			7.0	5.0	0.8	0.2	0.13	0.07
100 down			2.0	0.06			7.0	5.0	1.0	0.1	0.12	0.08

\* Maximum and minimum value over approximately  $\pm 50$  km.

<sup>†</sup> rms voltage difference between spheres.

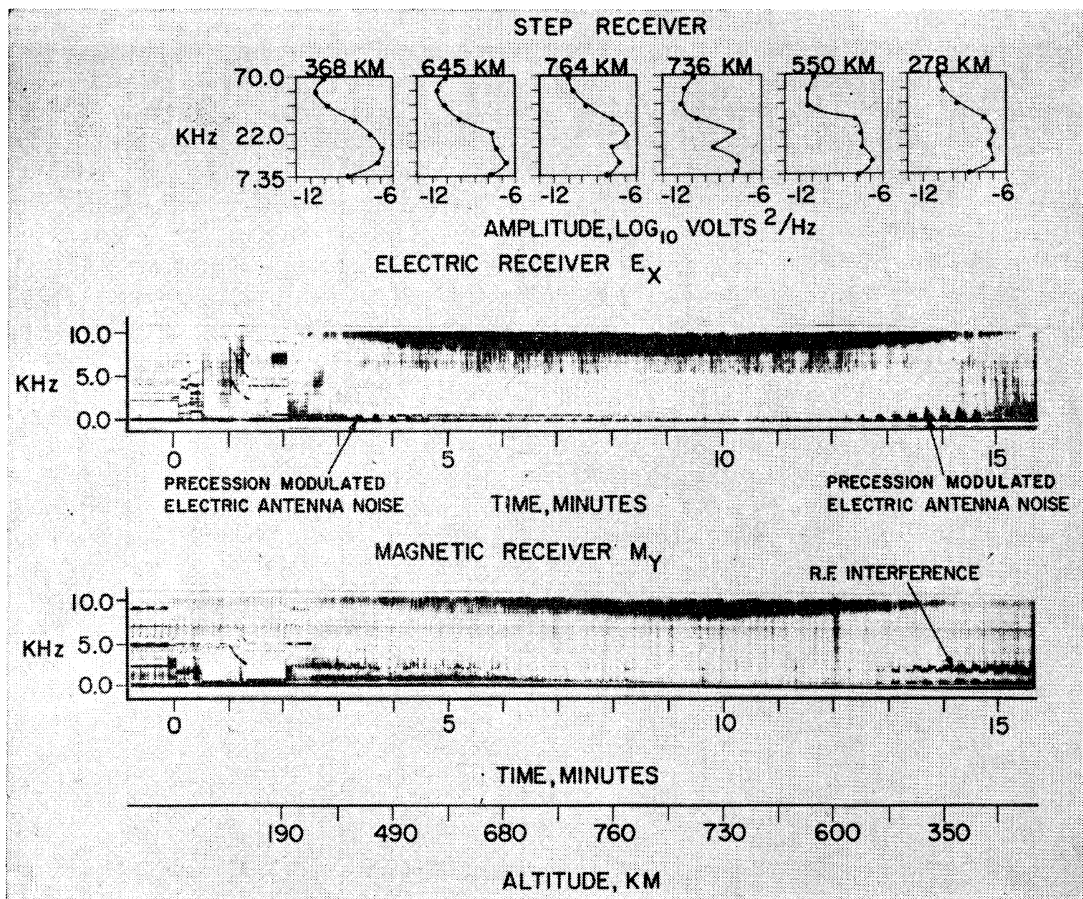


Fig. 3. Frequency spectra of electric and magnetic fields observed during the flight.

to 5 minutes and from 12.5 to 15 minutes as shown in Figure 3. The frequency-time spectrogram of this noise shows strong modulation at the precession period of the rocket (see Figure 3). The lo-band amplitudes of these noise bursts are very large, as much as 20 mv for the electric X and Y antennas and 8.0 mev for the TRW antennas. The peak intensity of these noise bursts varies systematically with altitude, having a maximum at about 275-km altitude and decreasing at higher altitudes. This noise is apparently electrostatic in origin since no comparable noise is observed in the magnetic receiver. Further analysis and discussion of this low frequency electric antenna noise are presented in section 6.

Besides the noise bands, hundreds of short fractional hop whistlers and 6 long hop whistlers were observed during the flight. The whistler signals are strongest on the magnetic re-

ceivers. In Figure 3 the randomly occurring vertical lines on the magnetic receiver spectrogram are whistlers.

*B. Impedance measurement results.* A frequency-time spectrogram of an impedance measurement sweep from the  $E_y$  receiver is shown in Figure 4. The driving signal for the impedance measurement is seen as an exponentially decreasing tone from 10 kHz to 20 Hz. For the first 0.5 second the impedance measurement stabilizes at 20 kHz. The sweep begins at 0.5 second, but the 20- to 10-kHz segment is not observable in the spectrogram.

The rising tone in Figure 4 is proportional to the logarithm of the impedance magnitude and represents a dynamic range of 100 kilohms to 10 megohms. The falling tone is linearly proportional to the phase angle between  $\pm 90^\circ$ . The impedance generally varies monotonically with frequency, from capacitive ( $-90^\circ$  phase

angle) at 20 kHz to resistive ( $0^\circ$  phase angle) at about 5 kHz and lower frequencies. The magnitude of the impedance at low frequencies (below 1 kHz) varies systematically with altitude and has a minimum of about 150 kilohms at 350-km altitude, increasing with increasing altitude to about 600 kilohms at apogee. Below the ionosphere the magnitude of the impedance at low frequencies increases to greater than 10 megohms. These impedance measurement results show that the input impedance of the preamplifiers for the Storey-type antennas (20-megohm resistance in parallel with a 10-pf capacitance) is sufficiently large that the potential drop through the antenna sheath is negligible. When these impedance values are scaled to the collecting area and dimensions of the TRW antenna it is found that, because of the large input capacity of the TRW preamplifiers (100 pf), the input impedance of the TRW preamplifier is considerably less than the impedance of the TRW antenna. Because the sheath impedance varies considerably

throughout the flight and because detailed calculations of the TRW antenna impedance are subject to many uncertainties, the amplitudes from the TRW antennas cannot be interpreted as ac potentials in the plasma without correcting for the generally unknown sheath impedance. Under some conditions, particularly at low altitudes, the uncertainties in the sheath impedance of the TRW antennas can cause an overestimation error by as much as a factor of 30 in Scarf's determinations of electric fields with the P-11 and OV3-3 satellites [Scarf *et al.*, 1965, 1966, 1967].

The impedance measurement sweep in Figure 4 is somewhat unusual in that when the sweep frequency is between about 1.0 and 2.0 kHz there is a large positive (inductive) perturbation in the phase angle, reaching a maximum of approximately  $+45^\circ$ . This perturbation occurs when the angle  $\theta_y$  between the electric Y antenna and the geomagnetic field is near  $180^\circ$ . Phase perturbations similar to those illustrated in Figure 4 occurred primarily at low

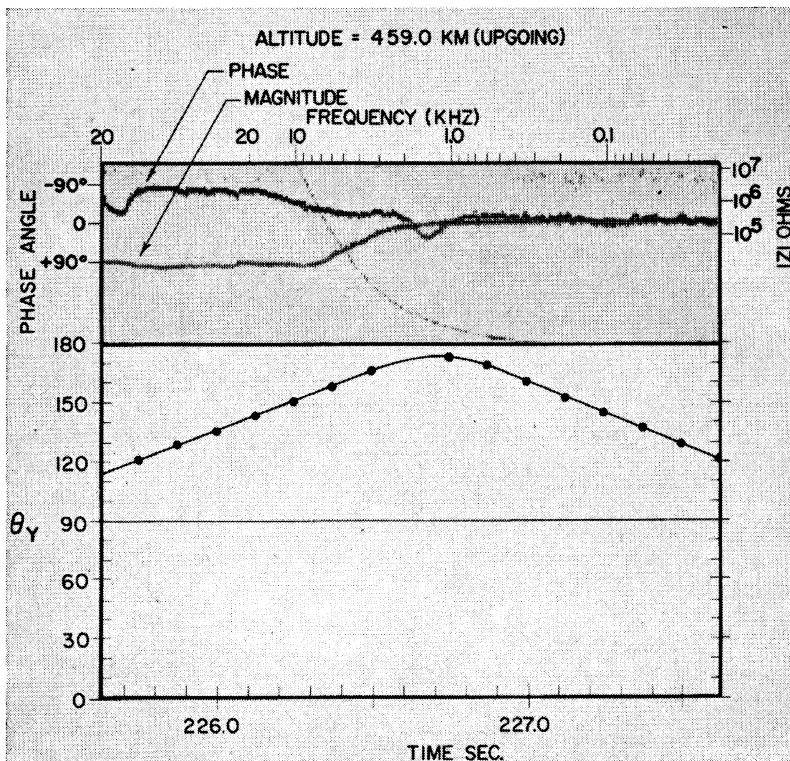


Fig. 4. Typical impedance measurement sweep.

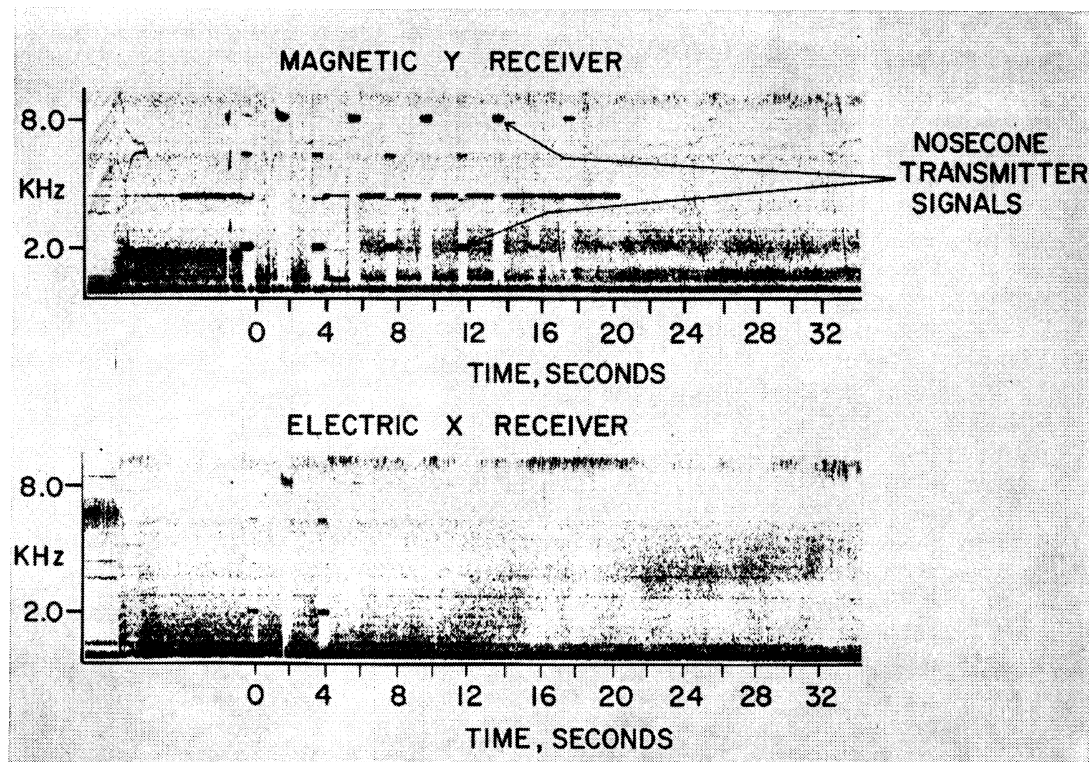


Fig. 5. Nosecone transmitter signals.

altitudes, below 500 km, whenever the  $E_y$  antenna was aligned nearly parallel to the geomagnetic field.

*C. Nosecone transmitter results.* Frequency-time spectrograms of the magnetic and electric fields from the nosecone transmitter are shown in Figure 5 as a function of time from the end of the first pulse at 2 kHz (harmonics of 2 kHz are also seen). The electric antennas and magnetic loops were not fully extended until after eight seconds in Figure 5. Because of the deceleration of the nosecone (see section 3), the separation velocity indicator cannot give the final separation velocity and distance. As yet radar records of the nosecone trajectory have not been analyzed to determine the separation distance.

Qualitatively in Figure 5 it is seen that the electric field signal is attenuated much more rapidly than the magnetic field signal. Pulses at 8 kHz can be seen past 28 seconds in the magnetic Y receiver, but only to 5 seconds in the electric X. From the energetics of nosecone ejection an upper limit of 2 m/sec can be

placed on the separation velocity. The transmitted magnetic signal is therefore observed to be less than 5 mV at a range of no more than 22 meters. Also, no radio noises or instabilities were observed to be stimulated by the nosecone transmitter at any time during the flight.

#### HIGH-FREQUENCY ELECTROMAGNETIC NOISE BAND

Figure 3 shows the general spectral characteristics of the high-frequency noise band observed between approximately 7.5 and 30 kHz. Since the noise band appears in both the electric and magnetic receivers, this noise is electromagnetic in nature.

From the three orthogonal loop antennas and the two crossed dipole antennas five wave field components can be measured to provide information on the field geometry and mode of propagation of the noise. In Figure 6 the band amplitudes in millivolts for the  $E_x$  and  $E_y$  receivers are compared with the angles  $\theta_x$ ,  $\theta_y$ , and  $\theta_z$  between the  $x$ ,  $y$ , and  $z$  payload axis and the geomagnetic field. This figure shows that the



high-frequency noise band is strongly modulated at the precession and spin rate of the payload. The sharp nulls in the electric field amplitude, about a factor of 5, occur when the corresponding electric antenna is nearly parallel to the geomagnetic field. Thus, the electric field of this noise is very nearly perpendicular to the geomagnetic field (within about  $\pm 10^\circ$ ). The deep spin modulation nulls in the electric field amplitude occur only when the spin axis is perpendicular to the geomagnetic field ( $\theta_z \approx 90^\circ$ ) and are almost absent during the portion of the precession cycle when  $\theta_z$  is not near  $90^\circ$ . This precession modulation of the depth of the spin modulation nulls in the electric field amplitude indicates that the electric field amplitude is azimuthally symmetric around the geomagnetic field and that the electric field is confined to a plane nearly ( $\pm 10^\circ$ ) perpendicular to the geomagnetic field.

A comparison of the spin modulation of the magnetic and electric hi-band amplitudes is illustrated in Figure 7. During the time interval of this comparison the spin axis was nearly perpen-

dicular to the geomagnetic field so that as the rocket spins the  $x$  and  $y$  axes alternately become aligned nearly parallel and perpendicular to the geomagnetic field. Figure 7 illustrates that when  $\theta_x$  approaches  $0^\circ$  or  $180^\circ$ , the  $M_x$  and  $E_y$  amplitudes have maxima while  $M_y$  and  $E_x$  exhibit minima, and conversely for  $\theta_y$  approaching  $0^\circ$  or  $180^\circ$ . The ratio of the maximum to the minimum amplitudes of the spin modulation is less for the magnetic field, about 1.4, than for the electric field, about 3.0. From the spin modulation of the magnetic field we can conclude that the wave magnetic field  $\mathbf{B}^{(1)}$  tends to be parallel to the geomagnetic field. It follows, therefore, that the wave normal direction  $\mathbf{K}$  of this noise tends to be perpendicular to the geomagnetic field, since Maxwell's equation  $\nabla \cdot \mathbf{B} = 0$  implies that  $\mathbf{K}$  be perpendicular to  $\mathbf{B}^{(1)}$ .

Three additional spectral features of this noise band have been noted. First, measurements of the lower cutoff frequency of the noise band from the spectrograms in Figure 3 have shown that the lower cutoff frequency is approximately ( $\pm 2\%$ ) proportional to the geo-

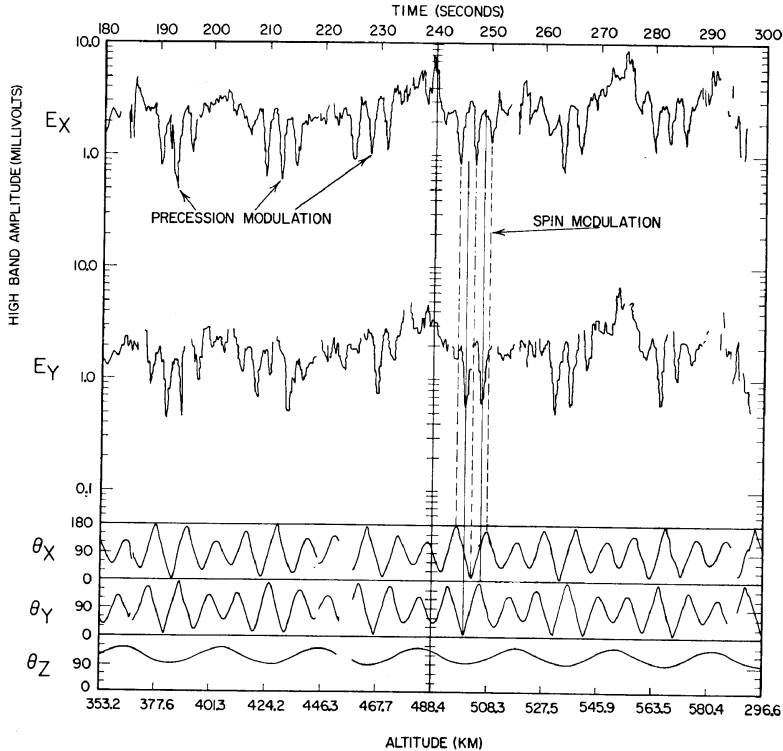


Fig. 6. Electric field spin and precession modulation of the high-frequency electromagnetic noise band.

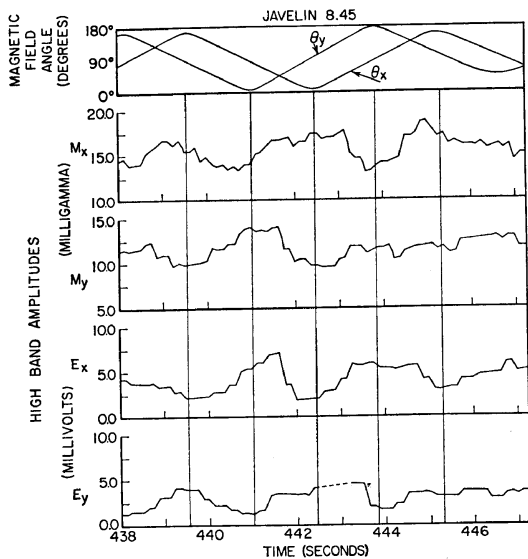


Fig. 7. Comparison of the electric and magnetic field spin modulation of the high-frequency electromagnetic noise band.

magnetic field strength. Second, the electric field of the noise band has a consistently lower cutoff frequency than the magnetic field. This cutoff frequency difference ranges from about 200 Hz at 200-km altitude to 500 Hz at apogee (763 km). Finally, higher resolution spectrograms of the noise band reveals that the noise band is not made up of steady 'white noise' but appears to be a superposition of many noise bursts occurring on a time scale of tens of milliseconds. On the electric field spectrograms many short duration (<100 millisecond) noise bursts are seen that extend several kHz below the noise band cutoff and appear to have a less well-defined cutoff at about 5.0 kHz. These noise bursts below the noise band cutoff are not observed on the magnetic field spectrogram.

This experiment with receivers and antennas capable of simultaneously measuring five of the six wave field components has provided unique information about the observed noise. The principal features of the high-frequency noise band can be summarized as follows. The noise band has a low-frequency cutoff, which decreases with increasing altitude approximately proportional to geomagnetic field strength; the upper frequency cutoff is approximately 30 kHz also decreasing with increasing altitude; the spectrum appears to be made up of many noise bursts, some of which extend below the lower cutoff

frequency of the electric field noise band; the noise is electromagnetic; the electric field cutoff frequency is lower than the magnetic field cutoff frequency; the wave electric field is in a plane very nearly perpendicular to the geomagnetic field; and the wave magnetic field tends to be parallel to the geomagnetic field, implying that the waves are propagating at large angles, nearly transverse, to the geomagnetic field.

*Discussion.* Some of the features of the high-frequency noise band observed on the Javelin 8.45 flight suggest that this noise band is identical to the lower hybrid resonance (LHR) noise observed by Barrington *et al.* [1963] and Brice and Smith [1964, 1965] with the electric dipole antenna on the Alouette 1 satellite. The principal feature of the Alouette 1 LHR noise is that the noise has a sharply defined lower cutoff frequency, typically from 4 to 15 kHz, which is believed to be the lower hybrid resonance frequency of the ambient plasma [see McEwen and Barrington, 1967]. LHR noise has also been observed with a magnetic loop antenna on the Injun 3 satellite [Gurnett, 1967], although with much less frequency than on Alouette 1.

The following points of comparison can be made between the LHR noise hypothesis and the high-frequency noise band observed on this rocket flight.

(1) In the altitude range of the Javelin 8.45 flight above about 300-km altitude, where the dominant ion is  $O^+$  and where the electron plasma frequency is greater than the electron gyrofrequency, the LHR frequency is proportional to the geomagnetic field strength in agreement with the observed variation in the lower cutoff frequency of the high frequency noise band.

(2) The computed LHR frequency for the above conditions varies from about 8.0 kHz at 300-km altitude to about 6.2 kHz at apogee (763 km), *always slightly less than* (about 10%) but very close to the observed cutoff frequency.

(3) The LHR frequency is an electrostatic resonance ( $E/B$  becomes infinite) for propagation perpendicular to the geomagnetic field, consistent with the observed large electric field, the difference in the cutoff frequencies of the electric and magnetic fields, and the evidence that the noise is propagating perpendicular to the geomagnetic field.

(4) Below about 300-km altitude where the electron plasma frequency is comparable with or less than the electron gyrofrequency the LHR frequency becomes proportional to the square root of the electron concentration, no longer proportional to the geomagnetic field strength, and decreases rapidly with decreasing altitude. No corresponding variation in the cutoff frequency of the high-frequency noise band is observed. Thus, below about 300-km altitude the observed cutoff of the high-frequency noise band *cannot* be the LHR frequency.

The observed systematic decrease in the lower cutoff frequency with increasing altitude suggests that this cutoff may simply be an accessibility condition for waves emitted by a source at higher altitudes. Reflection of down-going waves can indeed occur just below the lower hybrid resonance frequency for waves propagating nearly perpendicular to the geomagnetic field. Above about 300-km altitude, where the lower hybrid resonance frequency increases with decreasing altitude, this reflection

process could explain the observed cutoff near the lower hybrid resonance frequency. Below about 300-km altitude, where the lower hybrid resonance frequency decreases with decreasing altitude, the observed cutoff may be just the upper edge of the 'stop band' caused by lower hybrid resonance reflections at higher altitudes.

#### LOW-FREQUENCY ELECTRIC ANTENNA NOISE

Expanded frequency-time spectrograms of the precession-modulated electric antenna noise illustrated in Figure 3 are shown in Figure 8 for the electric X, electric Y, and TRW antennas. These spectrograms cover the period from about 12.5 to 14 minutes in Figure 3 during the down-going portion of the flight. The blank regions in the TRW spectrograms are periods when this receiver was switched to the magnetic Z antenna. The intensity cutoff at 650 Hz is due to the gain difference between the lo and hi bands.

Two distinct types of low-frequency electric antenna noise can be distinguished from these

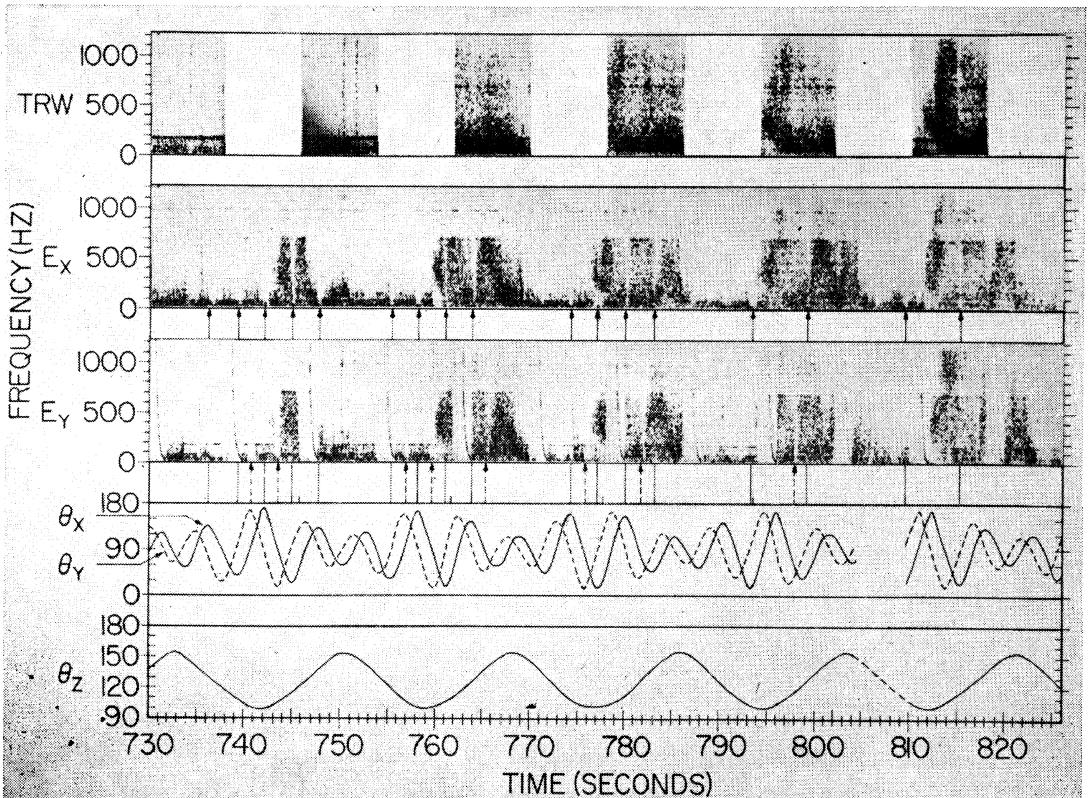


Fig. 8. Frequency spectra of the low-frequency electric antenna noise.

spectrograms: (1) a component having frequencies up to about 1 kHz, which is strongly modulated at the precession period of the rocket (hereafter referred to as precession modulated noise), and (2) a relatively steady noise below about 150 Hz, which is present with nearly constant amplitude throughout the flight. Neither of these noises is observed on the magnetic antennas.

As can be seen from Figure 3 the precession-modulated noise is only observed between about 250- and 500-km altitude. The upper frequency limit and intensity of this noise decrease systematically with increasing altitude. The precession modulation pattern of this noise consists of a period during which the noise is undetectable, followed by a rapid onset with the upper frequency limit of the noise initially rising very rapidly (see Figure 8). The 'envelope' of the frequency-time spectra of the noise burst is roughly symmetric about the center of the noise burst and is almost identical for all three antennas. During the downgoing portion of the flight the center of the noise burst leads the maximum in  $\theta_z$  by about  $\frac{1}{4}$  of a precession period (see Figure 8).

Spin modulation effects are much less pronounced than the precession modulation. The spin modulation observed, as can be seen from Figure 8, consists of rather sharp nulls at all frequencies occurring when the angle between the antenna axis and the geomagnetic field is a minimum. The spin modulation nulls occur when the antenna is aligned nearly parallel to the geomagnetic field.

Frequency-time structure on a time scale of a few tenths of a second can be seen that is not related to the rocket orientation. This fine structure is usually different for the three antennas. Generally the intensity of the noise increases toward lower frequencies.

The lo-band amplitudes of the electric X, electric Y, and TRW antennas are shown in Figure 9 for the upgoing portion of the flight between 2 and 5 minutes in Figure 3. The blank regions in the TRW amplitudes occur when this receiver is switched to the magnetic Z antenna. The maximum amplitude of the electric antenna noise occurs at an altitude of about 250 km for all three antennas, approximately 20 mv for the electric X and electric Y antennas and 8 mv for the TRW antenna. In contrast

to the downgoing portion of the flight, where precession modulation of the low-frequency electric antenna noise occurred at all altitudes, precession modulation was observed only above about 370 km on the upgoing leg. From Figure 9 it is seen that the precession-modulated amplitudes of the three electric antennas track very closely, with the  $E_x$  and  $E_y$  amplitudes generally being within about  $\pm 25\%$  and the TRW amplitudes usually being somewhat less than  $E_x$  or  $E_y$ , by a factor of from 1.5 to 3. The maxima in the precession-modulated amplitudes are seen to occur when  $\theta_z$  is a maximum ( $145^\circ$ ), and the nulls in the precession modulation occur when the spin axis is perpendicular to the geomagnetic field ( $\theta_z = 90^\circ$ ).

Spin modulation of the lo-band amplitudes can be seen at several points in Figure 9 and is much less pronounced than the precession modulation. The sharpest nulls in the spin modulation occur when the antenna axis is nearly parallel with the geomagnetic field, consistent with the spin modulation illustrated in Figure 8 for the downgoing portion of the flight.

Comparing the upgoing (Figure 9) and downgoing (Figure 8) portions of the flight, two principal differences are noted in the precession-modulated noise. First, precession modulation of the low-frequency noise did not occur during the upgoing portion of the flight until approximately one minute after nosecone separation, from about 220- to 370-km altitude in Figure 9. During the downgoing portion of the flight precession modulation was observed at all altitudes. Second, the phase of the precession-modulated noise relative to the phase of the angle between the spin axis and the geomagnetic field,  $\theta_z$ , is different for the upgoing and downgoing portions of the flight (compare Figures 8 and 9). Analysis of the angle between the  $z$  axis and the several coordinate system vectors indicates that the precession-modulated noise is in phase with the angle between the  $z$  axis and the  $V_1$  velocity. For both the upgoing and downgoing portions of the flight it is found that when the  $z$  axis is approximately parallel to the  $V_1$  direction no precession-modulated noise is observed, and when the angle between the  $z$  axis and  $V_1$  is a maximum the amplitude of the precession-modulated noise is also a maximum.

During the nulls in the precession modulation and during the portion of the flight above about 500-km altitude where the precession-modulated

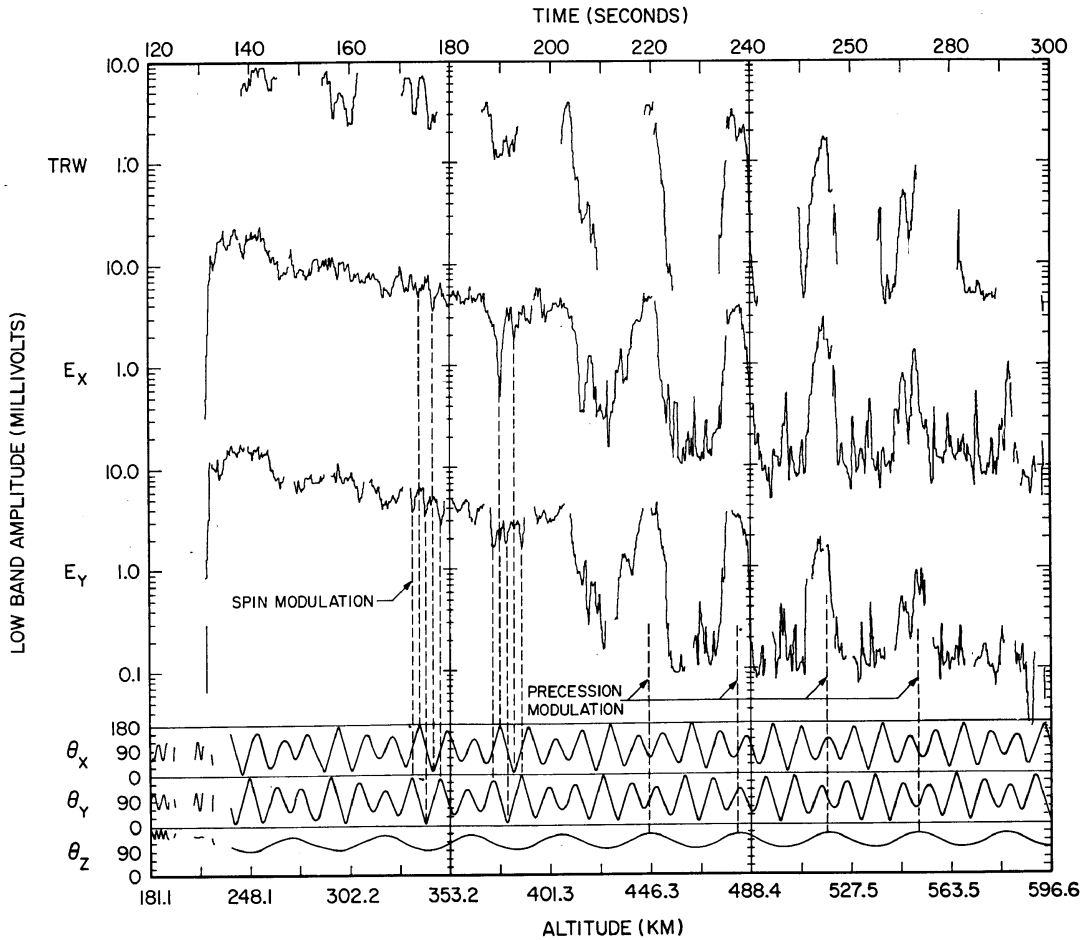


Fig. 9. Amplitude of the low-frequency electric antenna noise on the upcoming portion of the flight.

noise does not occur, the  $E_x$  and  $E_y$  lo-band amplitudes are about 0.1 mv, and the TRW lo-band amplitude is about 0.05 mv. These minimum noise levels, well above the receiver noise level, remain nearly constant throughout the flight and correspond to the steady noise observed below about 150 Hz in Figure 8.

This noise also has sharp spin modulation nulls occurring when the angle between the antenna axis and the geomagnetic field is a minimum.

*Discussion.* Electric antenna noise possibly similar to the precession modulation observed by this experiment has been reported by Scarf *et al.* [1965, 1966, 1967], using measurements from the 1964-45A and OV3-3 satellites, and by Iwai *et al.* [1966], using data from the L-3-2

sounding rocket. Because of the low frequency-time resolution of the 1964-45A and OV3-3 experiments it is difficult to determine whether the low-frequency electric antenna noises observed by Scarf near perigee are of the type observed with the Javelin 8.45 experiment.

Iwai *et al.* [1966], using data from the ELF-VLF electric field experiment on the L-3-2 sounding rocket, launched to an apogee altitude of 337 km, have reported the observation of intense ( $>0.1$  mv) periodic noise bursts in the frequency range from 0.5 to 3.5 kHz with maximum intensity at about 1.0 kHz near apogee. The modulation period of these noise bursts were believed to correspond to the spin and precession periods of the rocket (no orientation data were available). From Iwai's description it

appears almost certain that the noise observed with the L-3-2 experiment is the same as the precession-modulated noise observed with Javelin 8.45. Some of the common characteristics include: (1) maximum intensity in the frequency range below 1.5 kHz, (2) observed in the altitude range 200–500 km, (3) strong precession modulation, and (4) spin and precession modulation not consistent with a simple (cosine law) antenna pattern.

In considering the origin of these low-frequency electric antenna noises two key questions must be investigated; first, are the antenna noises in fact caused by ac electric fields in the surrounding plasma or could the noise be caused by fluctuations in the plasma properties (electron concentration, temperature, etc.) that affect the floating potential of the spherical antenna elements, and, second, are the electric fields or plasma fluctuations a natural phenomena in the ionosphere or are the noises caused by the interaction of the payload with the surrounding plasma?

Despite the considerable amount of data available from the Javelin 8.45 experiment these questions are by no means conclusively answered at the present time. Some of the present conclusions regarding the precession-modulated noise are summarized as follows:

(1) *Long wavelength electrostatic waves.* Several features of the Javelin 8.45 data suggest that if the precession-modulated noise is due to electrostatic waves in the ionosphere, then the wavelength of these waves cannot be substantially longer than the  $E_x$  or  $E_y$  antenna length ( $\sim 3.0$  meters). First, for long wavelengths the potential difference between the antenna elements is proportional to the cosine of the angle between the electric field and the antenna axis. The precession and spin modulation of the low-frequency electric antenna noise is not consistent with this simple cosine dependence. For example, since both the  $E_x$  and  $E_y$  antennas have nulls in the precession-modulated noise when the spin axis is approximately parallel to  $\mathbf{V}_\perp$  we must conclude that the electric field is polarized parallel to  $\mathbf{V}_\perp$ . However, one-half precession period later, when the noise is present, the  $E_x$  and  $E_y$  antennas show no evidence of spin modulation nulls when they are perpendicular to  $\mathbf{V}_\perp$ . Second, for long wavelengths the potential difference between the antenna elements is proportional to the length of the an-

tenna. This length dependence is not observed for the precession-modulated electric antenna noise. As can be seen from Figure 9 the noise amplitudes from the electric X and Y antennas and the TRW antenna are generally comparable (never more than a factor of 3 difference), even though their lengths differ by a factor of 6.5. Third, since the TRW antenna is sensitive to electric field components in both the X and Y directions the ac signals from the TRW receiver should correlate with the electric X and Y signals. A preliminary correlation study, performed by filtering each channel with identical filters ( $\sim 25$  cps bandwidth) and comparing the phases of the filtered signals, revealed *no* significant correlation between the precession-modulated noise from the TRW antenna and the electric X and Y antennas.

(2) *Doppler shift.* It is possible that the above facts could be reconciled if the precession-modulated noise is due to wavelengths sufficiently short that the fields at the electric X and Y antennas are essentially uncorrelated with the fields at the TRW antennas (i.e., wavelengths much less than about 3 meters). Except for the unlikely situation that the waves are propagating nearly perpendicular to the velocity vector it follows that the noise must be very strongly Doppler-shifted. For example, since the rocket velocity is about 3 km/sec, a wave with a wavelength of 1 meter is Doppler-shifted by 3 kHz. Since the bandwidth of the observed noise is generally less than about 1 kHz it is difficult to see how the short wavelength requirement can be reconciled with the observed bandwidth of the precession-modulated noise unless the wave vectors are precisely orientated to reduce the Doppler shift. These considerations, although by no means conclusive, suggest that there are considerable difficulties with interpreting the precession-modulated noise as ac electric fields in the ionosphere.

(3) *Noise generated by the motion of the payload.* Certain features of the precession-modulated noise suggest that this noise may be generated by the motion of the payload through the ionosphere. First, the precession modulation of the noise is controlled by the  $z$ -axis orientation of the rocket. In particular, the almost 'on-off' amplitude of the noise is correlated with the angle between the  $z$  axis and the perpendicular projection of the velocity vector  $\mathbf{V}_\perp$ . As discussed above, this dependence is difficult to understand in terms of nat-

urally occurring wave phenomena in the ionosphere. Since the last stage of the rocket remained attached to the payload it is possible that a turbulent wake from the rocket bottle (dimensions approximately 18 inches diameter by 4 feet long) may be causing the observed noise. It may be significant that, owing to the perturbation when the booms opened, the payload is flying more or less backward with the rocket bottle upstream in the  $V_{\perp}$  direction (see Figure 2). Thus the antennas tend to be in the wake region much of the time.

The second feature suggesting a wake effect is the fact that the precession-modulated noise was of a distinctly different character during the period approximately 1 minute after nosecone separation. During this period no precession modulation was observed (see Figure 9), and the noise amplitude was approximately 4 times the amplitude observed during the downgoing portion of the flight at the same altitude. This asymmetry between the upgoing and downgoing portions of the flight suggests that a wake from the nosecone, which was ejected forward along the velocity vector, may be producing some of the observed noise when the nosecone was close to the payload.

(4) *Antenna bias current.* Varying the sheath impedance by changing the antenna bias current would help resolve the question of whether electric fields or fluctuations in the plasma parameters could be causing ac noise in the floating potential of the spheres. Unfortunately, since the electron gun failed, this information is not available for this flight. It has been suggested (P. Kellogg, personal communication) that variations in the antenna bias current because of the changing rocket orientation may be causing the precession modulation of the low-frequency electric antenna noise. Since the average potential of the spheres relative to the payload shell was monitored, we have determined the maximum variation of the bias current to be about  $10^{-8}$  amp, considerably less than the ion current incident on the spheres. Also, the observed noise was the same on the insulated grid spheres ( $Ex$ ) as on the conducting spheres ( $Ey$ ). Thus, it seems unlikely that bias current variations could cause the observed modulation.

This experiment has provided a considerable amount of new information on ac electric and magnetic fields in the ionosphere and on the

performance of electric antennas in plasmas. Many questions, however, remain unanswered, particularly regarding the relationship of the lower hybrid resonance frequency to the lower cutoff frequency of the high-frequency noise band and the origin and nature of the low-frequency electric antenna noise.

*Acknowledgments.* We would like to express our appreciation to Dr. F. L. Scarf for providing the TRW electric fields experiment and for his helpful discussions.

We are very grateful to Mr. J. R. Cessna, Mr. R. D. Anderson, and Mr. J. A. Miller for their technical assistance in the design and construction of the payload and to Mr. N. Peterson, Mr. V. Laurie, and Mr. R. Plihal at the Sounding Rockets Branch of Goddard Space Flight Center for their assistance and advice.

This research was supported by the National Aeronautics and Space Administration under contract NSR-16-001-025 and grant NGR-16-001-043 and by the Office of Naval Research under contract Nonr 1509(06).

#### REFERENCES

- Barrington, R. E., J. S. Belrose, and D. A. Keeley, Very low frequency noise bands observed by the Alouette 1 satellite, *J. Geophys. Res.*, **68**, 6539, 1963.
- Brice, N. M., and R. L. Smith, A very low frequency plasma resonance, *Nature*, **203**, 926, 1964.
- Brice, N. M., and R. L. Smith, Lower hybrid resonance emissions, *J. Geophys. Res.*, **70**, 71, 1965.
- Gurnett, D. A., Satellite observations of VLF emissions and their association with energetic particles, *Department of Physics and Astronomy, University of Iowa, Iowa City, Iowa, Res. Rept. 67-53*, 1967.
- Gurnett, D. A., S. D. Shawhan, and G. W. Pfeiffer, Description of the Injun V VLF experiment, *Department of Physics and Astronomy, University of Iowa, Iowa City, Iowa, Res. Rept. 65-34*, 1966.
- Iwai, A., J. Otsu, and Y. Tanaka, The observation of ELF-VLF radio noise with sounding rockets L-3-2, K-9M-6, *Proc. Res. Inst. Atmospheric Sciences Nagoya University*, **13**, 1, January 1966.
- McEwen, D. J., and R. E. Barrington, Some characteristics of the lower hybrid resonance noise bands observed by the Alouette 1 satellite, *Can. J. Phys.*, **45**, 13, 1967.
- Scarf, F. L., G. M. Crook, and R. W. Fredricks, Preliminary report on detection of electrostatic ion waves in the magnetosphere, *J. Geophys. Res.*, **70**, 3045, 1965.
- Scarf, F. L., G. M. Crook, and R. W. Fredricks, Survey of VLF electric fields in the magnetosphere with the polar orbiting spacecraft, 1964-

45A, *Radio Sci.*, 1, (New Series). No. 8, August 1966.

Scarf, F. L., R. W. Fredricks, and G. M. Crook, Detection of electromagnetic and electrostatic waves on OV3-3, *TRW Systems Rept. 09485-6001-R000*, Redondo Beach, California, 1967.

Storey, L. R. O., Antenne Electrique Dipole Pour Reception TBF Dans, L'Ionosphere, *L'onde Electrique*, t. SLV, No. 465, December 1965.

(Received April 19, 1968;  
revised June 5, 1968.)